Mine Water and the Environment (2023) 42:312–329
https://doi.org/10.1007/s10230-023-00939-1

TECHNICAL ARTICLE

Evaluation of Water Inrush Vulnerability and Feasibility Analysis of Mining Under Rivers: A Case Study Involving the Jinjie Coal Mine in China

Aoshuang Mei[1,2] · Qiang Wu[1,2,3] · Yifan Zeng[1,2,3] · Yashuai Cui[1,2] · Di Zhao[1,2]

Received: 31 October 2022 / Accepted: 17 May 2023 / Published online: 7 June 2023

Abstract

The shallow groundwater of the Quaternary Salawusu Formation in China is distributed widely in the arid and semi-arid areas of northern Shaanxi and is an essential component of water supply and ecosystem maintenance there. To safely exploit the coal resources and protect the water resources, it is important to understand the impact of local high-intensity coal mining on such shallow groundwater. We used the "three maps—two predictions" method, the theory of equivalent mining height, and numerical simulations to evaluate the water inrush conditions for the 3–1 coal seam and to analyze the feasibility of backfill mining under the Qingcaojiegou and Hezegou Rivers. The results for the Jinjie coal mine showed that: part of the Quaternary porous phreatic aquifer and most of the J_2z weathered-bedrock pore–fissure confined aquifer are high-risk areas in the connectivity zoning map; there are large areas of strong or relatively strong water-abundant areas in the 3–1 coal seam roof, and; large areas in the southwest, northwest, and northeast parts of the coalfield are in high- and low-risk areas and face a serious threat of roof water inrush. Overall, it should be feasible to mine under these rivers, using backfill mining to effectively reduce the height of the water-flowing fractured zone and amount of surface subsidence.

Keywords Water hazard in coal mines · Method of three maps-two predictions · Numerical simulation · Water-preserved mining · Backfill mining

Introduction

With the exhaustion of coal resources in central and eastern China, the focus of coal mining has shifted gradually westward (Bai et al. 2019; Gui and Lin 2016; Li and Wu 2019; Mu et al. 2020; Zeng et al. 2022). In 2021, the coal output in western China was 3.54 billion tonnes (t), accounting for 85.8% of the national total and an important component of China's economy. However, in the western region, evaporation typically far exceeds rainfall, the proportion of arable land to woodland is below the national average, and groundwater is mostly scarce, making this an ecologically fragile region (Zhang et al. 2009; Zhu et al. 2022). The contradiction between the mining of coal and the fragile ecological environment in western China has become increasingly prominent (Zeng et al. 2022; Zhao et al. 2022a).

Research has been done on how to balance resource usage and environmental protection in western China, and the concepts of "coal–water" double-resources mine construction, green mining, and water-preserved mining have been successively proposed (Fan 2005; Miao and Qian 2009; Wu and Li 2009). Coal mining has led to the destruction of aquifers and aquicludes, increased the rates of mine water inflow, and introduced safety hazards. Mining has also destroyed groundwater resources and affected the surface ecosystem (Zeng et al. 2023; Zhao et al. 2022b).

Regarding roof water hazard prediction, the representative prediction methods include "three top layers" theory, "key stratum" theory, mutation theory pan-decision analysis, and "two zones" study, which focus on the abundance of

✉ Yifan Zeng
zengyf@cumtb.edu.cn

1 National Engineering Research Center of Coal Mine Water Hazard Controlling, China University of Mining and Technology (Beijing), Beijing 100083, China

2 College of Geoscience and Surveying Engineering, China University of Mining and Technology (Beijing), Beijing 100083, China

3 University of Mining and Technology (Beijing) Inner Mongolia Research Institute, Ordos 017000, Inner Mongolia, China

water in roof aquifers and the inrush mechanisms (Booth et al. 2000; Qian et al. 1996; Zeng et al. 2016). Given the issues involved in mining under waterbodies, countries generally require longwall technology for coal seams that meet certain conditions, while backfilling or room-and-pillar mining methods are used under different conditions. For example, Great Britain, Japan, Chile, and Canada require that when the minimum cover layer thickness exceeds 60 m, 93 m, 70 m, and 55 m, respectively, room-and-pillar or backfilling mining methods can be used for extraction (Booth and Bertsch 2002; Islam et al. 2009; Kim et al. 1997; Shen 2017).

Because most coal mines in China are subjected to limited pumping tests that do not incorporate multisource information such as aquifer hydraulic characteristics, it is difficult to accurately evaluate the true water abundance (Zeng et al. 2017). Based on the GIS (geographic information system) multisource information fusion technique of "three maps—two predictions," we used a multisource geologic information composite study to assess the risk of roof water hazard based on the available data. This avoids the limitations and one-sidedness of conclusions caused by the heterogeneity and anisotropy of aquifers and other factors (Wu et al. 2015b; Zeng et al. 2017).

Northern Shaanxi is in the contiguous area of Shanxi, Shaanxi, and Inner Mongolia in western China, an ecologically fragile area (Lv et al. 2019; Wang et al. 2019; Zhou et al. 2019). The Quaternary Salawusu Formation phreatic aquifer is 5785 km^2 in area, accounting for more than half of the total area of northern Shaanxi. The widely distributed Quaternary Salawusu Formation phreatic aquifer is an important water-supply aquifer in the area, playing a vital role in the stability of local industrial and agricultural production and the normal life of residents, and it is a precious water resource for maintaining the healthy development of surface vegetation and the ecological environment (Yang et al. 2016). The high-intensity exploitation of coal resources, which affects aquifers in the Salawusu Formation, not only restricts production safety but also causes groundwater wastage and massive damage to the fragile ecological environment.

The Jinjie coal mine in northern Shaanxi has an annual production capacity of more than 1×10^7 t. Because of the shallowness of the coal seam, aquicludes are missing in some areas, resulting in an average inflow of 3200 m^3/h and a maximum inflow of 5499 m^3/h of mine water, which severely threatens the safe production of coal and has a large impact on shallow water resources. Therefore, we used the "three maps—two predictions" technology to study the risk of water inrush from the aquifer of the coal seam roof of the Jinjie coal mine and then formulate a scientific mining method for the high-risk zone.

Geological and Hydrogeological Conditions

The Jinjie coal mine in Yulin City in Shaanxi Province is located at the northern end of the Loess Plateau and the southeastern margin of the Mu Us Desert, a mainly aeolian landform. The central and western parts of the coalfield belong to the Tuwei river basin, a tributary of the Yellow River, and mainly include the Qingcaojiegou and Hezegou rivers, both of which flow perennially and discharge into the Tuwei River southwest of the coalfield. The northeastern corner of the coalfield belongs to the Wulanmulun River basin, the first tributary of the Yellow River (Fig. 1).

Most areas around the Jinjie coal mine are covered by aeolian sand. From oldest to youngest, the strata comprise the Middle Jurassic Yan'an Formation (J_2y) and Zhiluo Formation (J_2z), the Neogene Baode Formation (N_2b), the Quaternary Lishi Formation (Q_2l), the Upper Pleistocene Salawusu Formation (Q_3s), and the Holocene aeolian sand (Q_4^{eol}) and alluvion (Q_4^{al}) (Fig. 1 and Supplemental Fig. S-1). The J_2y is the coal-bearing stratum of the Jinjie coal mine and can be divided into five intermediate cycles numbered from bottom to top as the first to fifth sections. The main mining coal seam, 3–1, is located at the top of the third section of the Yan'an Formation (J_2y^3). The stratigraphic dip angle is less than 1°, there are no folds or magmatic activity, there are only three minor normal faults, and the geological structure is not complex.

The main aquifers above the 3–1 coal seam in the Jinjie coal mine are a Quaternary porous phreatic aquifer (i.e. the Quaternary aquifer) and a J_2z weathered-bedrock pore–fissure confined aquifer (i.e. the J_2z aquifer). The former includes a valley alluvium phreatic aquifer (Q_4^{al}) and a Salawusu Formation phreatic aquifer (Q_3s), which have strong hydraulic connection. The hydraulic conductivity of the Quaternary aquifer is 0.813–4.760 m/day, and the specific capacity is 0.060–1.722 L/(m·s), which indicates that its water abundance ranges from weak to strong. The hydraulic conductivity of the J_2z aquifer is 0.142–0.882 m/day, and the specific capacity is 0.040–0.666 L/(m·s), which indicates that its water abundance ranges from weak to moderate. The primary aquicludes are the Quaternary Lishi Formation loess and the Neogene Baode Formation laterite. Because of the development of ancient gullies during the deposition of the loess and laterite in the coalfield, the thickness of these two layers varies considerably, with some sections being extremely thin and even missing in large areas.

Materials and Methods

Three Maps—Two Predictions

There are two necessary conditions for the occurrence of water inflow or inrush in a coal seam roof, i.e. that: (i) the water-flowing fractured zone formed by mining connects with the overlying aquifer and (ii) is sufficiently rich in water to cause a mine water inflow or inrush (Zeng et al. 2017). The "three maps—two predictions" method addresses the three major issues of roof water inrush, i.e. groundwater source, groundwater passage(s), and the water-bearing nature of the overlying aquifer (Wu et al. 2015a, b; Zeng et al. 2017). The "three maps" part refers to the connectivity zoning map, the water-abundance zoning map, and the comprehensive zoning map of roof water inrush conditions, while the "two predictions" part involves segmenting the working face and predicting the overall water inflow before and after the roof aquifer is grouted.

The connectivity zoning map indicates whether the roof thickness exceeds that of the water-flowing fractured zone: if the fracture is not connected to an aquifer, then the area is defined as relatively safe; if the fracture is connected to an aquifer, then there is a risk of water inflow or inrush in the area. The main factors controlling the water abundance index are determined using the hydrogeological data collected in the study area, and the water abundance elements are constructed using GIS multisource information fusion. All normalized subthematic maps are superimposed by GIS software, and then the relative importance (weight) of each control factor in each overlapping region is calculated by the analytic hierarchy process (AHP). This allows us to obtain the water-abundance zoning map. By superimposing the connectivity zoning map and the water-abundance zoning map, the comprehensive zoning map of roof water inrush conditions is obtained.

In this study, the empirical formula for estimating the height of the water-flowing fractured zone was revised with the measured height to create the connectivity zoning map. Factors such as aquifer thickness, specific capacity, hydraulic conductivity, core recovery ratio, and ratio of brittle and plastic rock were used to generate the water-abundance zoning map.

Theory of Equivalent Mining Height

Mining height is a major factor in rock movement and surface deformation. In backfill mining, the backfilling mass body is compacted by the backfill material and the roof subsidence, which is equivalent to reducing the mining height; the height of the water-flowing fractured zone also decreases (El-Nashaar et al. 2006; Guo et al. 2014; Zhang et al. 2015, 2016). The equivalent mining height H_z of backfill mining (Li et al. 2022) is:

$$H_z = h_t + h_q + h_y \tag{1}$$

where h_t is the amount of roof subsidence known in advance, h_q is the unfilled height, and h_y is the amount of compressed filling body, which can be obtained by:

$$h_y = \eta(h - h_t - h_q) \tag{2}$$

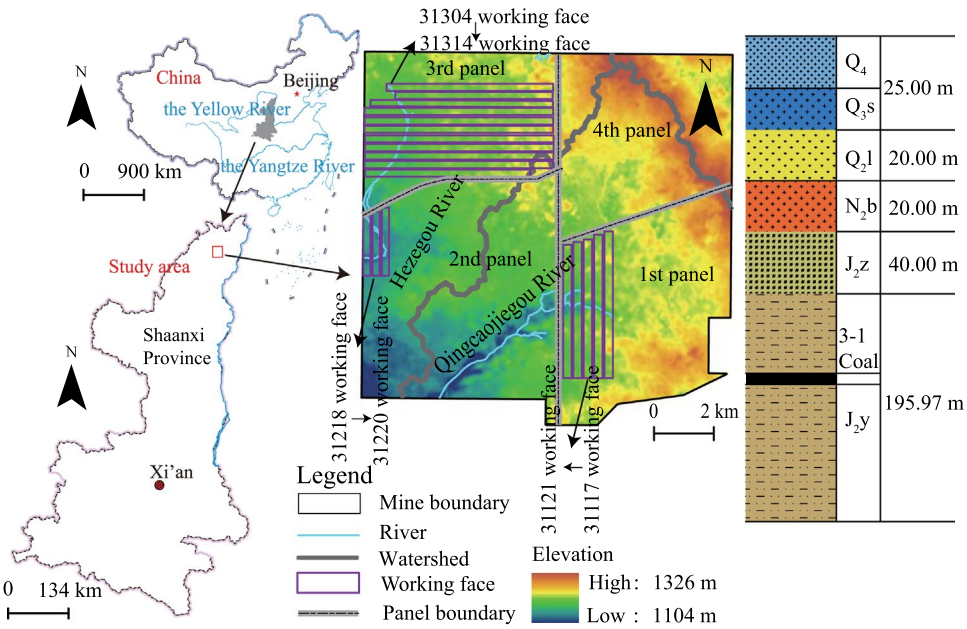

Fig. 1 Geographical location and strata of Jinjie coal mine

where h is the total mining height after backfill mining, and η is the compression ratio of the filling body and depends on porosity:

$$\eta = k_0 - k_n \tag{3}$$

where k_0 and k_n are the porosities of the solid backfill after initial and final compaction, respectively. Hence, we have H_z as:

$$H_z = h_t + h_q + \eta(h - h_t - h_q) \tag{4}$$

The average thickness of the coal seams under the river at the Jinjie coal mine is 3 m. Practice has shown that the compression ratio of paste after filling is typically 1–2%; to be conservative, we used a compression ratio of 2%. Empirically, the amount of roof subsidence was known in advance to be 0.24 m. The unfilled height is typically 50–100 mm, taken conservatively to be 0.1 m.

Numerical Simulation

FLAC3D (Fast Lagrangian analysis of continua) is three-dimensional (3D) finite-difference software that can simulate the 3D structural stress characteristics and plastic flow of soil, rock, and other materials (Bergado and Teerawattanasuk 2008). The actual structure is fitted by tuning the polyhedral elements in the 3D mesh, and linear or nonlinear constitutive models can be used for the elemental materials. Under the action of an external force, the mesh can deform and move accordingly as the material yields and flows. FLAC3D uses an explicit Lagrangian algorithm and a hybrid discrete partitioning technique to simulate material plastic failure and flow accurately (Rajeev and Kodikara 2011). Because there is no need to form a stiffness matrix, it is possible to solve large-scale 3D problems with less computer memory (Mase and Hashiguchi 2009).

In this study, we use FLAC3D to model the height of the water-flowing fractured zone at equivalent mining heights based on the regional geological environment of the 3–1 coal seam under surface rivers in the Jinjie coal mine. The working faces involved were 31,304–31,309, 31,310–31,314, 31,117–31,121, and 31,218–31,220 (Fig. 1). The length of the computational model for each set of working faces was 280 m and the width was 200 m, i.e. x = 280 m and y = 200 m. Based on borehole exposures, z-direction measurements were taken at 143.32 m, 121.92 m, 84.66 m, and 124.00 m. The physical and mechanical parameters of the rocks used in the calculations were obtained from the results of tests on the mechanics of rocks taken from the Jinjie coal mine (Tables 1, 2, 3 and 4).

Results and Discussion

Connectivity Zoning Map.

The lithology of the 3–1 coal seam is dominated by medium- and fine-grained sandstone with some coarse-grained sandstone, and the empirical formula for estimating the height of the mining-induced fracture zone in medium-hard rock was chosen according to the Specification for Coal Pillar Retention and Coal Mining in Buildings, Water, Railways and Main Roadways (State Administration of Work Safety 2017). Measurements of the height of the water-flowing fractured zone in the first panel of the Jinjie coal mine show that the maximum height was 45.72 m, and the mining thickness of the coal seam was 2.72 m. The calculated and measured values of the maximum height of the water-flowing fractured zone were compared; the correlation coefficient was 1.17292. Based on this, the empirical formula was revised as:

$$H_{li} = \frac{1.17292 \times 100 \sum M}{1.6 \sum M + 3.6} + 5.6 \tag{5}$$

where H_{li} [m] is the height of the water-flowing fractured zone and M [m] is the cumulative mining thickness. Using the revised formula, the height of the water-flowing fractured zone in the coalfield caused by 3–1 coal mining was calculated to exceed 40 m, with a maximum height of 61.83 m. This height enters the J_2z aquifer and locally connects to the Quaternary aquifer.

The thicknesses of the overlying strata from the 3–1 coal seam roof to the floors of the Quaternary aquifer and the J_2z aquifer were evaluated separately, and the height of the water-flowing fractured zone was compared to divide the connectivity zone. GIS stacking calculations were used to obtain connectivity zoning maps for the Quaternary aquifer and the J_2z aquifer within the 3–1 coal seam roof (Fig. 2).

In Fig. 2a, the whole of the third and fourth panels is relatively safe. In the first panel, only the relatively high-risk local section of the water-flowing fractured zone near the source of the Qingcaojiegou river on the west side can connect to the Quaternary aquifer. In the second panel, the relatively high-risk area is large and located mainly under the Qingcaojiegou river and nearby areas.

In Fig. 2b, the relatively high-risk area is considerably larger than the relatively safe area. The first, second, and fourth panels of the Jinjie coal mine are essentially relatively high risk, as is the third panel with the exception of some relatively safe areas in its northwest corner. In addition, some minor relatively safe areas are also distributed sporadically in the first and fourth panels.

Table 1 Physical and mechanical parameters of coal seam and rock mass in working faces 31,304–31,309

Lithology	Bulk modulus (GPa)	Shear modulus (GPa)	Cohesion (MPa)	Internal friction angle (°)	Tensile strength (MPa)	Density (kg/m^3)
Medium sandstone	0.028	0.025	0.002	17	0	2050
Silt and silty sand	0.019	0.017	0.004	20	0	1950
Siltstone	0.29	0.21	0.49	37	0.18	2390
Medium sandstone	2.683	2.18	4.37	34.9	1.83	2290
Gritstone	0.886	0.662	4.92	30.95	1.45	2390
Siltstone	3.267	2.548	4.31	36.6	1.62	2440
Fine sandstone	2.514	2.28	3.46	37	1.36	2460
Siltstone	3.267	2.548	4.31	36.6	1.62	2440
3–1 coal seam	2.8	1.701	2.05	36.5	0.737	1300
Fine sandstone	2.514	2.28	4.68	37.85	1.82	2470

Table 2 Physical and mechanical parameters of coal seam and rock mass in working faces 31,310–31,314

Lithology	Bulk modulus (GPa)	Shear modulus (GPa)	Cohesion (MPa)	Internal friction angle (°)	Tensile strength (MPa)	Density (kg/m^3)
Aeolian sand	0.01	0.008	0.004	17	0	2050
Silt and medium sand interbed	0.02	0.18	0.003	38	0	1950
Medium sandstone	0.33	0.38	0.49	43.2	0.18	2290
Siltstone	3.267	2.548	4.68	37.85	1.82	2470
Fine sandstone	2.514	2.28	4.31	36.6	1.62	2440
Siltstone	3.267	2.548	3.46	37	1.36	2460
3–1 coal seam	2.8	1.701	2.05	36.5	0.737	1300
Siltstone	3.267	2.548	4.68	37.85	1.82	2470

Table 3 Physical and mechanical parameters of coal seam and rock mass in working faces 31,117–31,121

Lithology	Bulk modulus (GPa)	Shear modulus (GPa)	Cohesion (MPa)	Internal friction angle (°)	Tensile strength (MPa)	Density (kg/m^3)
Alluvial deposit	0.017	0.015	0.05	17	0	1600
Loess	0.028	0.03	0.2	26	0	1800
Fine sandstone	0.29	0.21	0.49	37	0.18	2390
Medium sandstone	2.351	1.755	1.2	43	0.891	2280
Siltstone	2.333	1.971	2.6	41.5	1.6	2450
3–1 coal seam	2.8	1.701	2.05	36.5	0.737	1300
Fine sandstone	2.409	2.186	2.8	40	1.64	2280

Because the thicknesses of the loess and laterite aquicludes vary considerably, some aquiclude regions even disappear, and there are permeable "skylights" connecting the porous aquifer and the weathered-bedrock aquifer in the coalfield (Fig. 3). Therefore, it was necessary to revise the Quaternary aquifer by adding these skylight areas that allow the two aquifers to communicate, especially in the high-risk zones (Fig. 4).

Water-Abundance Zoning Map

Main Factors

Based on the available data, we determined that the main factors affecting the water abundance of the 3–1 coal seam roof aquifers were the aquifer thickness, specific capacity, hydraulic conductivity, core recovery ratio, and ratio of brittle and plastic rock.

Table 4 Physical and mechanical parameters of coal seam and rock mass in working faces 31,218–31,220

Lithology	Bulk modulus (GPa)	Shear modulus (GPa)	Cohesion (MPa)	Internal friction angle (°)	Tensile strength (MPa)	Density (kg/m^3)
Sand	0.028	0.025	0.002	17	0	2050
Sandy mudstone	0.29	0.21	0.49	37	0.18	2600
Siltstone	1.739	1.524	2.6	41.5	1.6	2450
Medium sandstone	3.048	2.477	3.4	41	2.12	2530
Siltstone	3.5	3.175	3.5	40.5	1.45	2400
3–1 coal seam	2.8	1.701	2.05	36.5	0.737	1300
Fine sandstone	2.514	2.28	4.68	37.85	1.82	2470

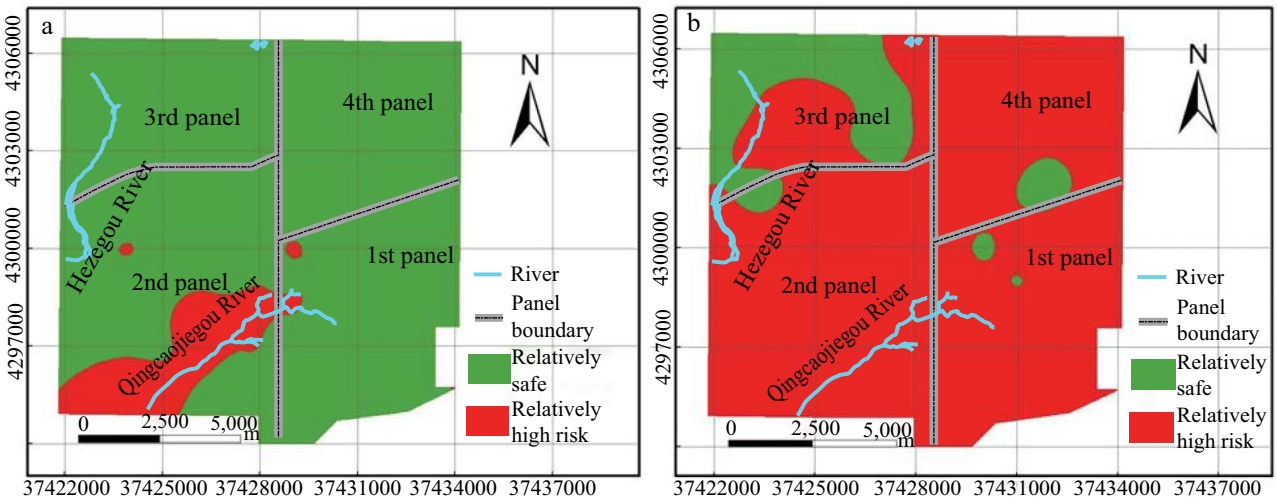

Fig. 2 Connectivity zoning maps for 3–1 coal seam to overlying aquifers: **a** Quaternary aquifer; **b** J_2z aquifer

Under certain conditions, the thicker the thickness of an aquifer, the greater its water abundance. The thematic maps of aquifer thickness (Supplemental Fig. S-2) show that the Quaternary aquifer is thick along the Qingcaojiegou River, medium in the northwest corner of the coalfield and along the Hezegou River, and relatively thin in other areas, while the thickness of the J_2z aquifer increases gradually along the line of the Qingcaojiegou River to the sides. This means that overall, the aquifer is thick in the north, of medium thickness in the southeast, and relatively thin along the Qingcaojiegou River in the southwest, along the Hezegou River in the west, and near the coalfield boundary in the east.

The specific capacity is the water inflow rate when the water level in the well is lowered by one meter during the pumping test. This is an essential metric for comparing aquifer water capacity: typically, the greater the specific capacity, the greater the aquifer's water abundance. From the thematic maps of specific capacity (Supplemental Fig. S-3), the flow from the Quaternary aquifer is larger in the southern part of the coalfield, decreases gradually northward, and is moderate at the northwest corner of the coalfield. The specific capacity of the J_2z aquifer increases gradually from the east and south to the northwest.

The hydraulic conductivity indicates the difficulty of fluid passage through the pore skeleton and can also reflect aquifer water capacity. Generally speaking, the greater the hydraulic conductivity, the greater the permeability of the rock and the water abundance of the aquifer. From the thematic maps of hydraulic conductivity (Supplemental Fig. S-4), that of the Quaternary aquifer is larger in the southwest of the coalfield and decreases gradually to the northeast, while that of the J_2z aquifer essentially increases from south to north.

The core recovery ratio is the ratio of the length of the core taken by the drill to the corresponding length of the actual drill hole, which can reflect the completeness of the rock mass. Typically, the lower the core recovery ratio, the higher the likelihood of connected cracks and the stronger the water abundance. From the thematic map of the core recovery ratio (Supplemental Fig. S-5), that of the J_2z aquifer is large in the east and northwest of the coalfield,

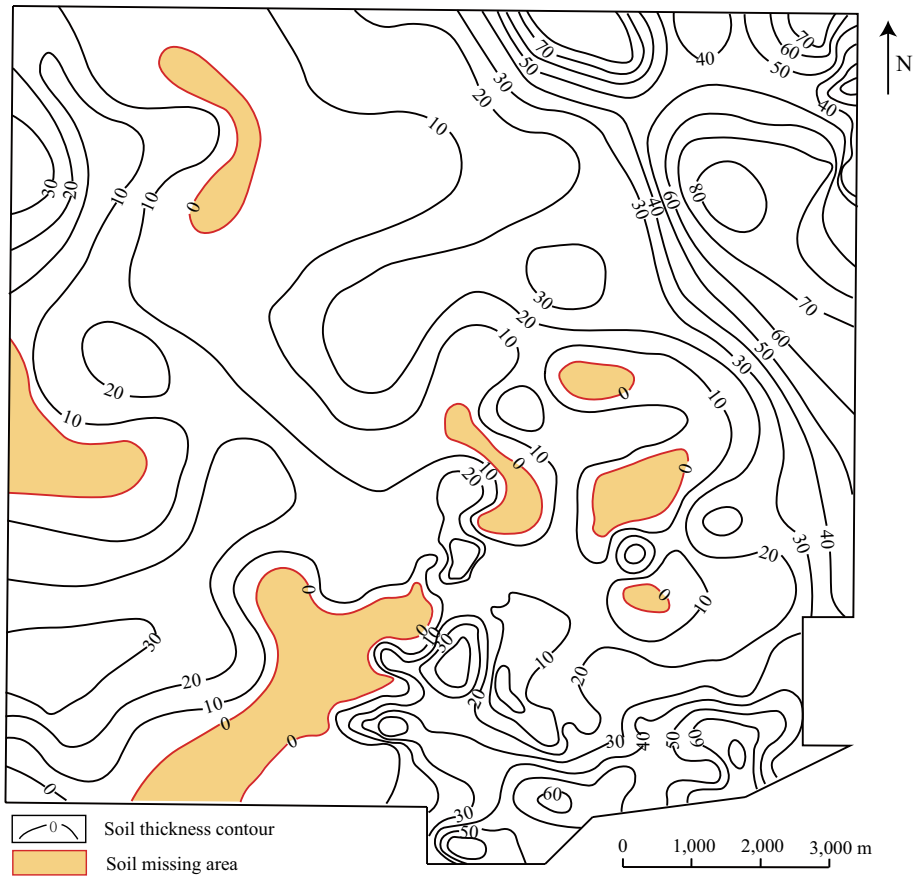

Fig. 3 Soil thickness contour map

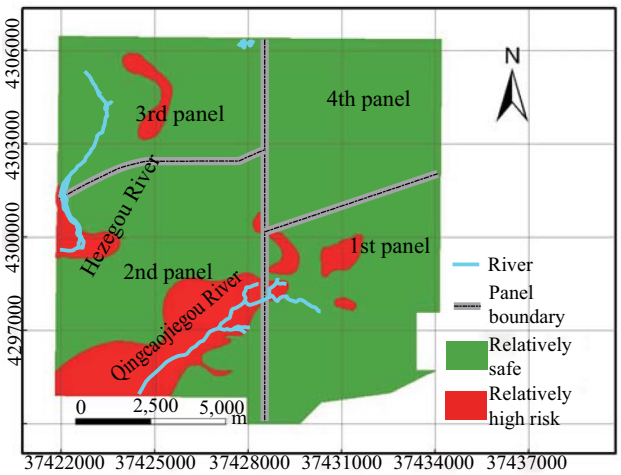

Fig. 4 Connectivity zoning map for Quaternary aquifer revised by adding "skylights"

indicating that the rock stability is superior in this region, with few connected cracks in the rock mass. The low core recovery ratio in other areas indicates that the rock there is less stable and the possibility of connecting cracks in the rock mass is high, which requires attention during mining.

The ratio of brittle and plastic rock can be used as an index to judge the permeability of an aquifer. In general, the larger the ratio of brittle and plastic rock, the larger the permeability of the aquifer and its water abundance. From the thematic map of the ratio of brittle and plastic rock (supplemental Fig. S-6), the ratio for the J_2z aquifer typically increases along the northeast–southwest diagonal to the sides. The ratio of brittle and plastic rock is larger in the northwest corner of the coalfield, moderate in the western and southeastern corners, and relatively minor in the other regions.

Weights of Controlling Factors

The AHP model is divided into three levels to reflect the multivariate information of aquifer water abundance. At the target level of the model (level A), the goal is to evaluate the aquifer water abundance. The aquifer and hydraulic field reflect the hydraulic properties of the aquifer, and the mode of influence must be reflected by the specific factors associated with it; this is the intermediate link to solve the problem, i.e. the subcriteria level (level B) of the model. Each specific piece of multivariate geographic information

constitutes the decision-making level of the model (level C), which allows the decision problem to be analyzed (Fig. 5a).

The relative importance of each factor is evaluated by: (i) analyzing the information that contributes to the aquifer water abundance, (ii) the opinions of experts, and (iii) the "1–9 and reciprocals" method (Saaty 1977). Each piece of information is scored quantitatively, and the judgment matrix of AHP evaluation of aquifer water abundance in the coal seam roof is constructed. The calculated weights of the controlling factors after the matrix operations are given in Table 5.

To make the multivariate geological information comparable and convenient for systematic analysis, the data for each piece of geological information were normalized to remove the restriction of different physical dimensions. All the controlling factors correlated positively with water abundance, and therefore maximum normalization was used:

$$Ai = \frac{x_i - min(x_i)}{max(x_i) - min(x_i)} \tag{6}$$

where Ai represents the dimensionless data, x_i represents the raw data, and $max(x_i)$ and $min(x_i)$ represent the maximum and minimum values, respectively. The water-abundance evaluation model for the Quaternary aquifer in the coal-seam roof of the coalfield is:

$$CI = \sum_{k=1}^{n} W_k \cdot f_k(x,y) = 0.33 \times f_1(x,y) + 0.5 \times f_2(x,y) + 0.17 \times f_3(x,y) \tag{7}$$

where CI is the water-abundance index, n is the number of factors, k is the serial number of the factors, W_k is the weight of the kth factor, $f_k(x,y)$ is the normalized value of the kth factor, and x and y are geographical coordinates.

Following the procedure described above, we also constructed a hierarchical structural model for the water-abundance evaluation of the J_2z aquifer (Fig. 5b); the calculated weights of the controlling factors are given in Table 6.

All the controlling factors correlated positively with water abundance except for the core recovery ratio. Therefore, minimum normalization was used for the core recovery ratio:

$$A_i = \frac{max(x_i) - x_i}{max(x_i) - min(x_i)} \tag{8}$$

where Ai represents the dimensionless data, x_i represents the raw data, and $max(x_i)$ and $min(x_i)$ represent the maximum and minimum values, respectively. The water-abundance evaluation model for the J_2z aquifer in the coal-seam roof of the coalfield is:

Table 5 Weighting of controlling factors for Quaternary aquifer

Controlling factor	Aquifer thickness	Special well discharge	Hydraulic conductivity
Weighting (*Wi*)	0.33	0.5	0.17

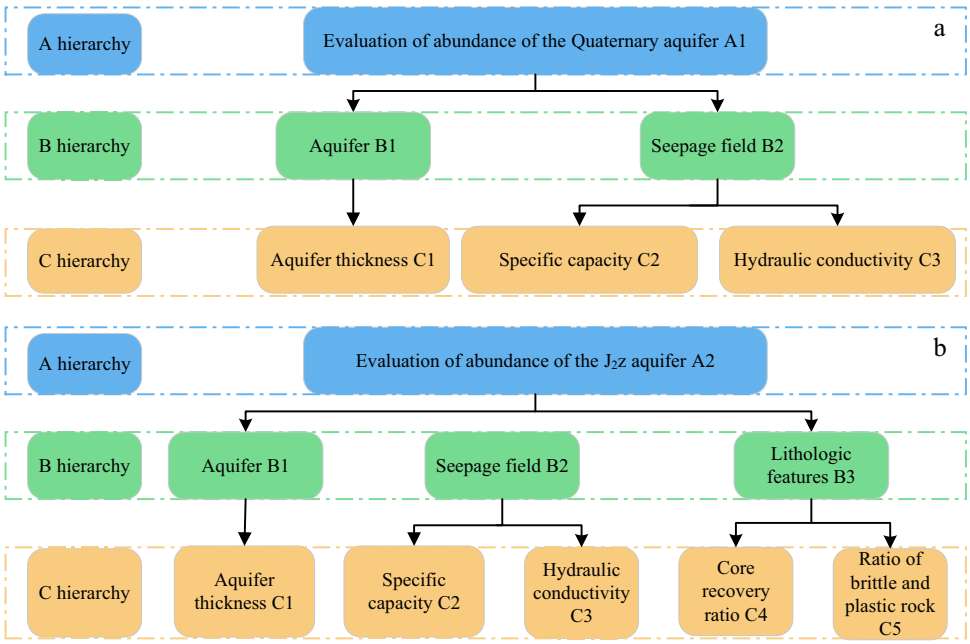

Fig. 5 Analytic hierarchy process (AHP) models of water abundance: **a** Quaternary aquifer; **b** J_2z aquifer

$$CI = \sum_{k=1}^{n} W_k \cdot f_k(x,y)$$
$$= 0.25 \times f_1(x,y) + 0.375 \times f_2(x,y) + 0.125 \times f_3(x,y) + 0.125 \times f_4(x,y) + 0.125 \times f_5(x,y) \quad (9)$$

where CI is the water-abundance index, n is the number of factors, k is the serial number of the factors, W_k is the weight of the kth factor, $f_k(x,y)$ is the normalized value of the kth factor, and x and y are geographical coordinates.

Water-Abundance Zoning

In the water-abundance evaluation model, GIS was used to superimpose the thematic maps of the controlling factors to obtain the water-abundance zoning maps of the Quaternary and J_2z aquifers (Fig. 6). To facilitate the application of zoning results during production, the whole area was divided into five subregions with different levels of water abundance using the natural breaks (Jenks) method (Aditian et al. 2018; Kazakis and Voudouris 2015; Roy et al. 2019).

Figure 6a shows that the strong and relatively strong water-abundant areas of the Quaternary aquifer in the roof of the 3–1 coal seam are located mainly in the southwest and northwest corners of the coalfield, including the area along the Qingcaojiegou River in the second panel and the central and northern parts of the third panel; these are the red and orange areas. Moderate water-abundant areas are

Table 6 Weighting of controlling factors for J_2z aquifer

Controlling factor	Aquifer thickness	Special well discharge	Hydraulic conductivity	Core recovery ratio	Ratio of brittle and plastic rock
Weighting (*Wi*)	0.25	0.375	0.125	0.125	0.125

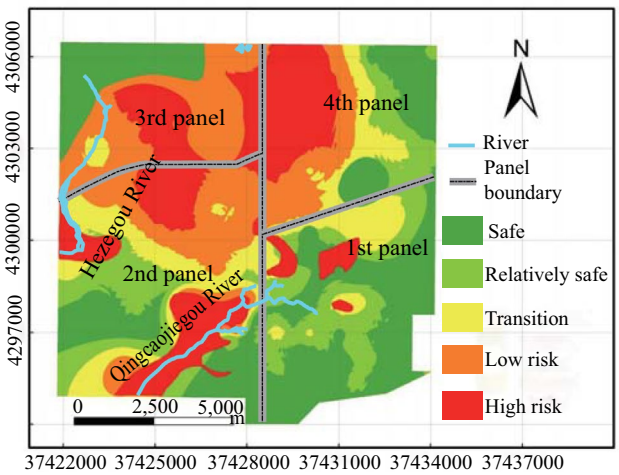

Fig. 7 Comprehensive zoning map of roof water inrush conditions

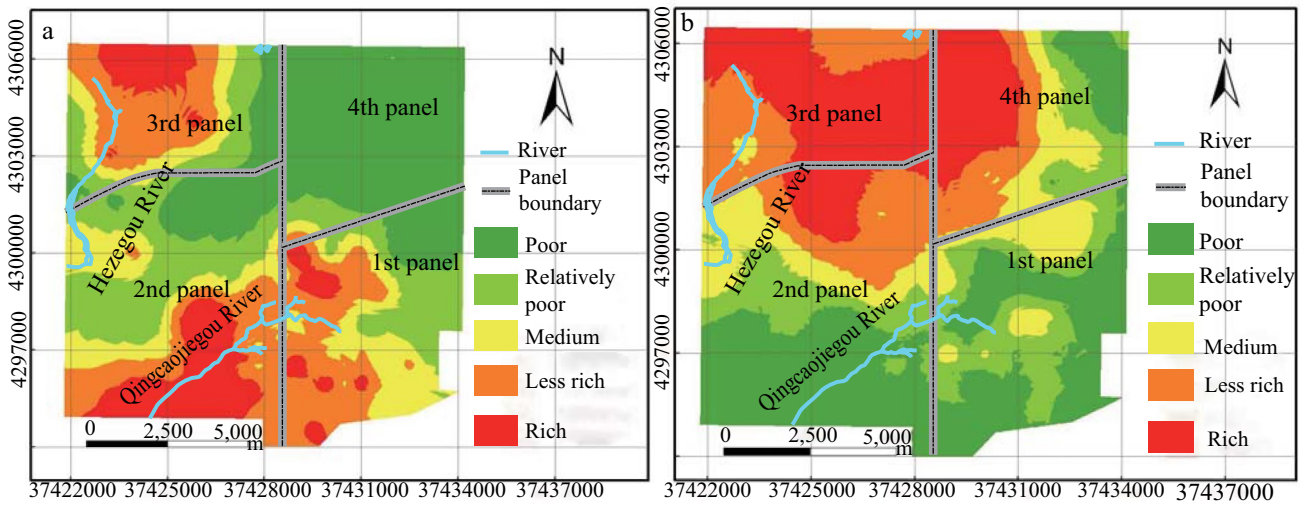

Fig. 6 Water-abundance zoning maps: **a** Quaternary aquifer; **b** J_2z aquifer

Table 7 Main methods for coal mining under rivers

Method	Advantages	Disadvantages	Feasibility
Full caving	Simple mining process, strong recovery rate, low coal loss, excellent economics	Severe perturbations to surrounding rock, extensive surface motion and deformation	The bedrock in this area is thin, and the development height of the water-flowing fracture zone spreads into the overlying aquifer, making this method unsuitable for use
Overburden-separation grouting	Significantly reducing surface settling effectively delays the rate of surface settling, with minor effects on other factors	This method is not yet mature	The coal-seam mining depth is shallow, and the overburden-separation position will not be very apparent and may not even produce separation, making this method unsuitable for use
Safety coal pillars	Typically, this method does not add additional drainage to the mine and does not require switching coal mining methods	Large loss of coal resources	It would be necessary to alter the layout of the mining works in order to exploit the coal resources separated by the rivers on either side, making this method unsuitable for use
River diversion	The most effective way to alter the water supply	The problem of river diversion involves a wide area, and large amounts of engineering and investment	Comprehensive planning and arrangements should be made based on the topography of mining areas and the development needs of industrial and agricultural production and construction, making this method unsuitable for use
Room-and-pillar	Mine development to prepare for minimal work, quick coal, less equipment investment, flexible face relocation, minimal roadway pressure, low level of damage to overlying rock	Coal pillars do not have long-term stability, and the coalfield has low recovery rates and poor ventilation conditions	Coal pillars without long-term stability are the biggest potential danger, and safety issues make this method unsuitable for use
Backfill mining	Filling in mined areas with backfilling material supports overlying formations, prevents rock movement, effectively controls surface subsidence, and improves resource recovery	Complicated mining and backfilling processes, higher mining costs	Relatively cheap pastes can be selected for backfilling, and paste-backfilling mining is one of the key technologies of the Green Mining Technology System in coal mines. For the ecological protection of Qingcaojiegou and Hezegou river, this method should be adopted

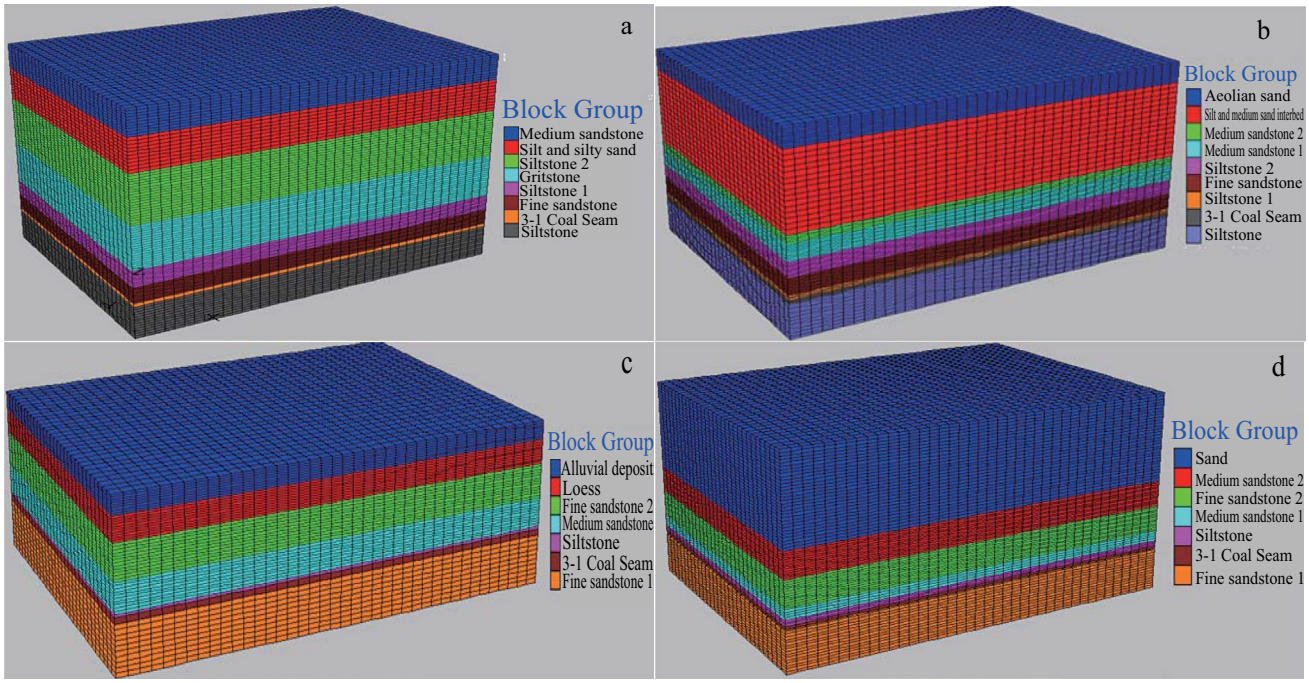

Fig. 8 Numerical computation models for four sets of working faces: **a** working faces 31,304–31,309; **b** working faces 31,310–31,314; **c** working faces 31,117–31,121; **d** working faces 31,218–31,220

distributed mainly along the edges of the strong water-abundant areas, and there is a tiny area in the middle of the west side of the coalfield; these are the yellow areas. The weak and relatively weak water-abundant areas are located mainly in the northeastern part of the coalfield and some areas in its middle; these are the green areas. Most of the areas in the fourth panel have weak water-abundance, and the other three panels have small portions of weak or relatively weak water-abundant areas. The Quaternary aquifer runoff direction in the study area is mainly from the north and east to the Qingcaojiegou and Hezegou Rivers; Fig. 6a shows that the evaluation results conform to this.

Figure 6b shows that the strong and relatively strong water-abundant areas of the J_2z aquifer are located mainly in the north and northwest of the coalfield, including most of the third panel and the west portion of the fourth panel; these are the red and orange areas. The moderate water-abundant areas are distributed mainly along the edge of the stronger water-abundant area; these are the yellow areas. The weak and relatively weak water-abundant areas are located mainly at the southern and eastern edges of the coalfield; these are the green areas. The underground runoff direction of the J_2z aquifer water in the study area is mainly from the north of the Qingcaojiegou River to the Hezegou River basin; Fig. 6b shows that the evaluation results conform to this.

Based on the above results, it can be seen that there is a large area of strong or relatively strong water-abundance in the Quaternary and J_2z aquifers in the coalfield. The overall trend of variation in aquifer water abundance is fundamentally consistent with the trends in aquifer thickness, specific capacity, hydraulic conductivity, and ratio of brittle and plastic rock and is basically opposite to that of the core recovery ratio. The shift trend of water-abundance is essentially consistent with the influence of the various controlling factors on aquifer water abundance.

Comprehensive Zoning Map

The water-flowing fractured zone created by mining the 3–1 coal seam at the Jinjie coal mine has resulted in the leakage of some areas of the Quaternary aquifer and much of the J_2z aquifer. Therefore, comprehensive zoning maps of the two aquifers were obtained by superimposing the connectivity zoning map and the water-abundance zoning map using ArcGIS software (Zeng et al. 2017). According to the principle of maximum risk, the ultimate comprehensive zoning map of roof water inrush conditions was obtained by superimposing the comprehensive zoning maps of the two aquifers (Fig. 7).

It can be seen from Fig. 7 that large areas in the second, third, and fourth panels of the coalfield are at high or low risk and therefore face a serious roof-water hazard threat. Because water-flowing fractured zones have developed to the surface in some places, we recommend enhanced

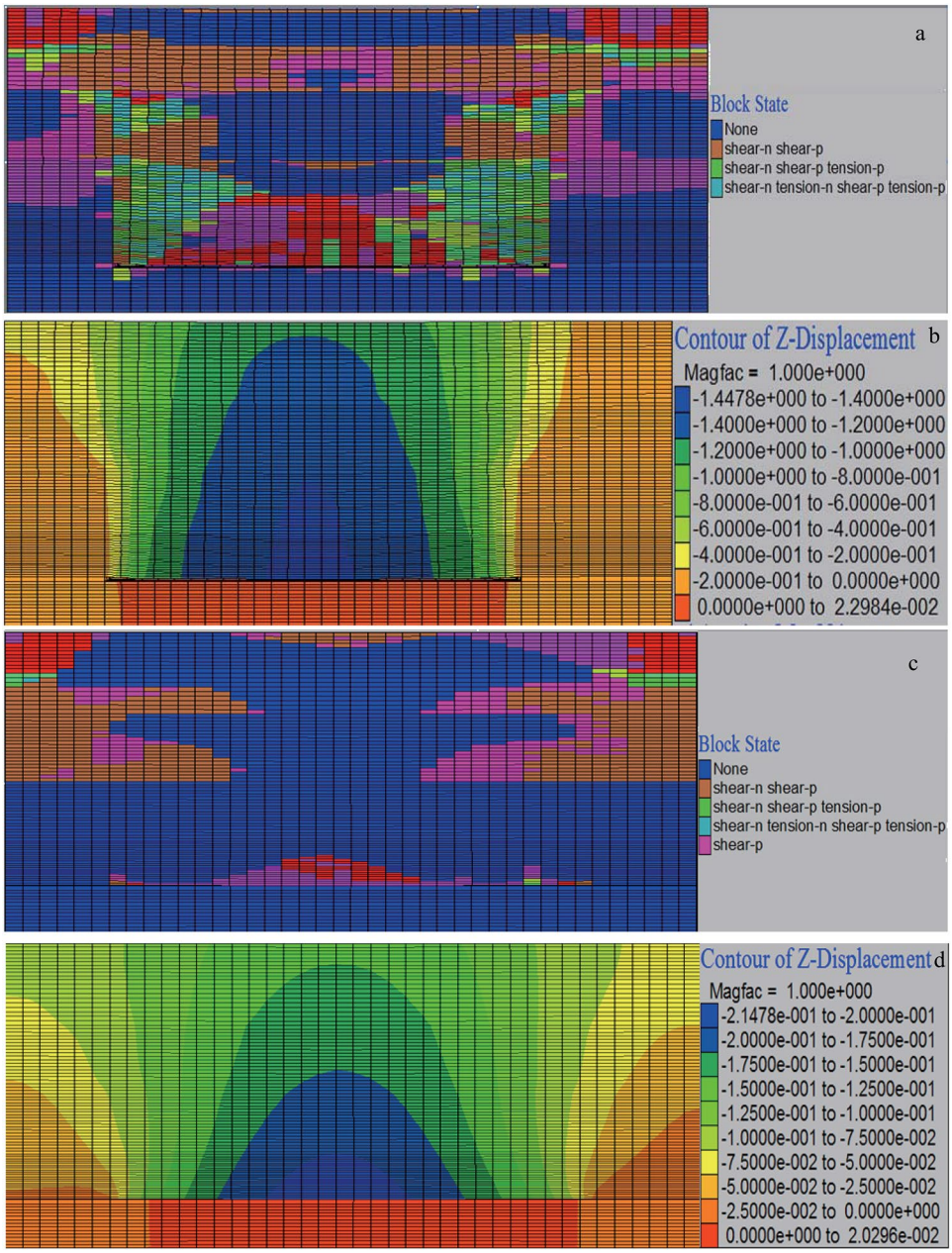

Fig. 9 Mining effects for working faces 31,304–31,309: **a** failure area of full caving; **b** vertical deformation of full caving; **c** failure area of backfill mining; **d** vertical deformation of backfill mining

inspection of surface crack damage in high-risk areas and the timely filling and intensive treatment of cracks. During mining, pre-mining borehole drainage can be conducted using two methods, i.e. underground drainage and ground drainage. The roof aquifer of the 3–1 coal seam is shallow, so surface drainage can be used if conditions permit; if the ground is not suitable, then underground drainage can be used instead. In danger zones, the two drainage methods can be combined to drain or reduce the aquifer water level, reduce the intensity of water inflow to the mining face, reduce the drainage burden, and achieve safe mining of the working face.

In addition, the areas beneath the Qingcaojiegou and Hezegou Rivers are at high risk. Improper mining there is prone to water inrush accidents, which would affect safe production and lead to wasted water resources, further threaten human drinking water and crop irrigation, and ultimately lead to the collapse of the entire fragile ecological environment. Consequently, a feasibility analysis should be carried out before mining below these rivers.

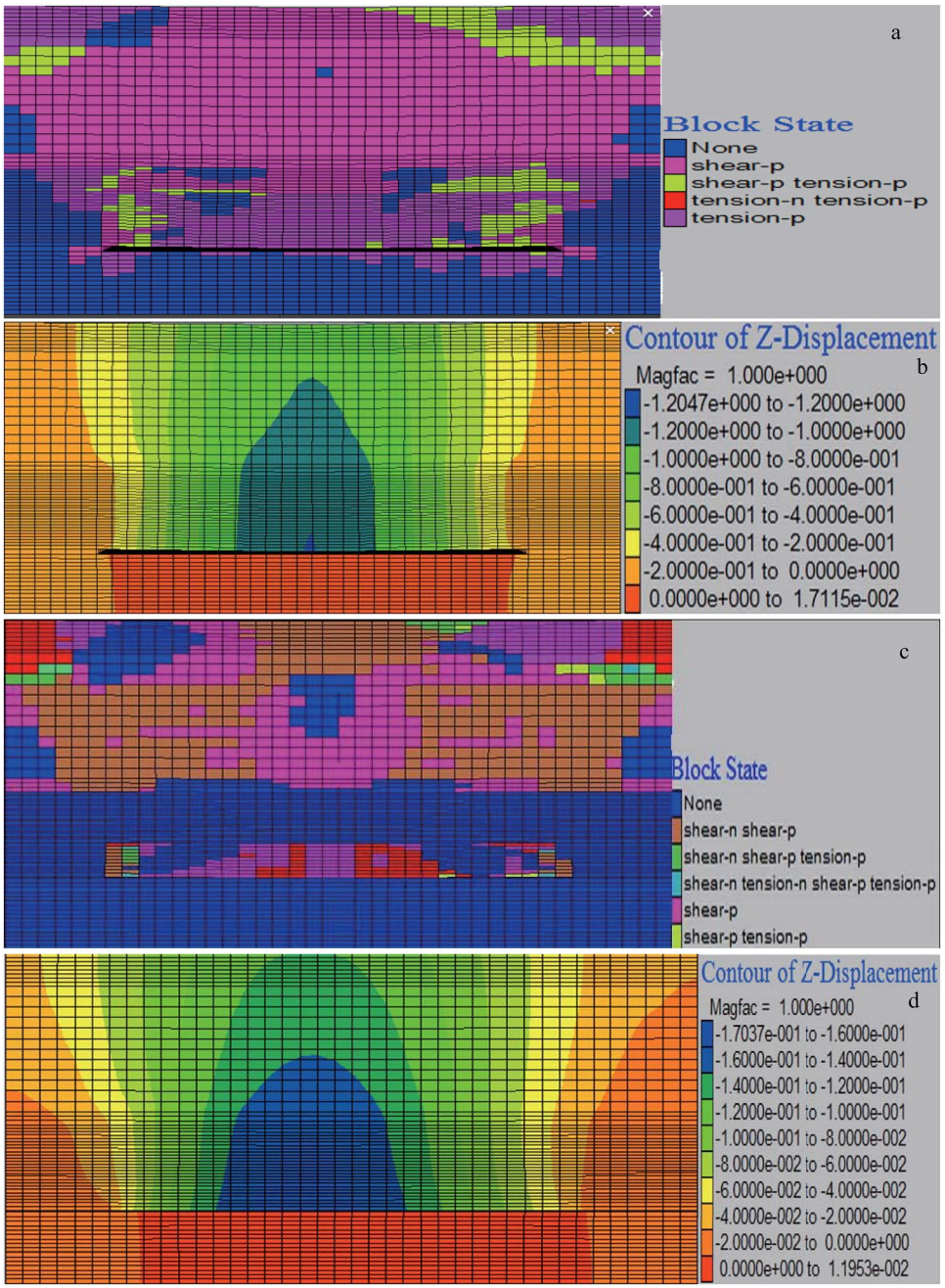

Fig. 10 Mining effects for working faces 31,310–31,314: **a** failure area of full caving; **b** vertical deformation of full caving; **c** failure area of backfill mining; **d** vertical deformation of backfill mining

Safe Mining Method

Height of Waterproof Coal (Rock) Pillar

According to the relevant provisions for the protective layer thickness of waterproof coal (rock) pillars in the Specification for Coal Pillar Retention and Coal Mining in Buildings, Water, Railways and Main Roadways, the protective layer for the Jinjie coal mine should be six times the mining thickness (State Administration of Work Safety 2017). The average mining thickness of the coal seam under the rivers of the coalfield is 3 m, and thus the protective layer thickness should be 18 m. From the revised formula [Eq. (5)], the height of the water-flowing fractured zone was calculated as 47.49 m, and the height of the waterproof coal (rock) pillars mined under the Quaternary groundwater and rivers was calculated as 65.49 m.

Selection of Mining Method

At present, the main methods for mining under water bodies are full caving, overburden-separation grouting, safety coal pillars, river diversion, room-and-pillar, and backfill

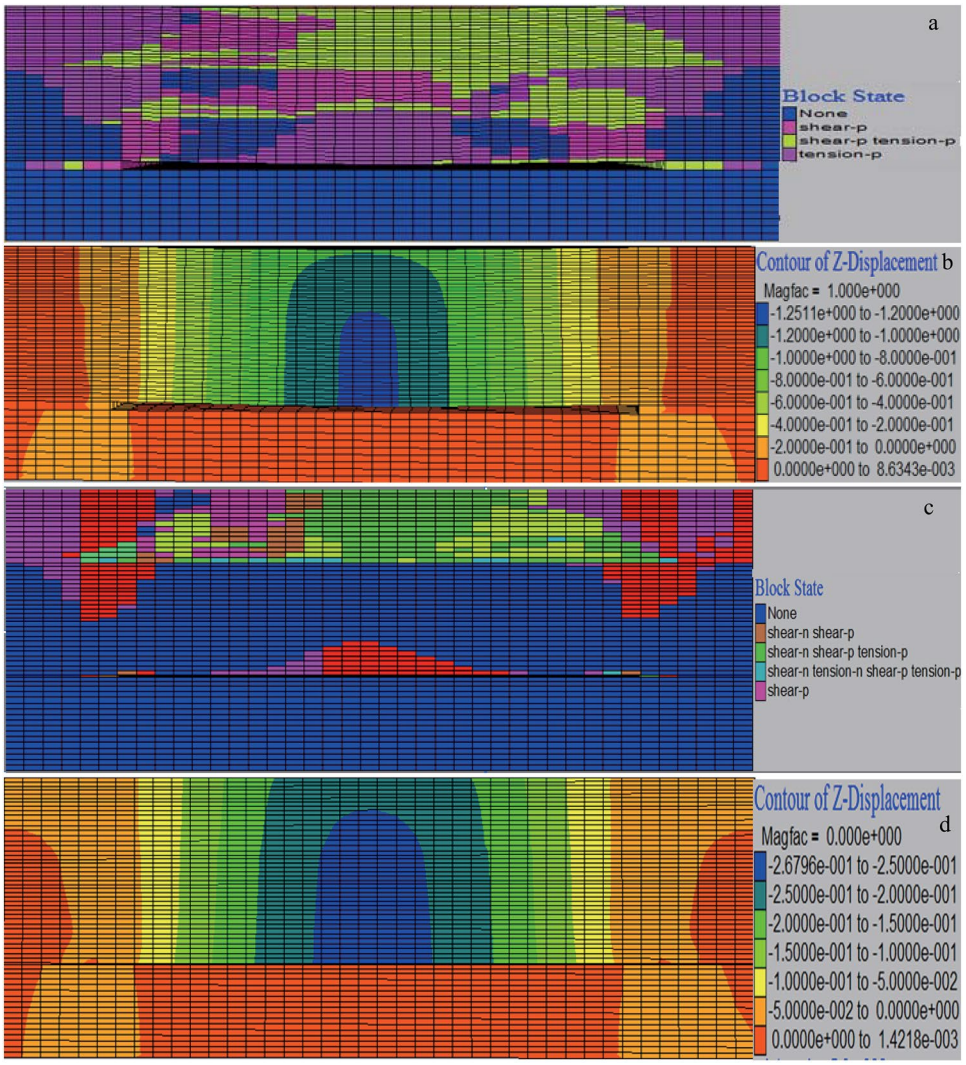

Fig. 11 Mining effects for working faces31117–31,121: **a** failure area of full caving; **b** vertical deformation of full caving; **c** failure area of backfill mining; **d** vertical deformation of backfill mining

mining (Chen et al. 2016; Esterhuizen et al. 2011; Flatley and Markham 2021; Ji et al. 2022; Wen et al. 2019; Zhang et al. 2018; Zhao et al. 2022c; Zheng et al. 2022; Zhou et al. 2017) (Table 7).

According to the present mining practices at the Jinjie coal mine, if longwall and backfill mining methods are used to mine under the rivers, then relatively cheap paste can be selected for backfilling. Moreover, from the perspective of local ecological environmental protection, backfill mining was selected for feasibility analysis. Using the established equivalent mining height formula for paste filling [Eq. 4], the equivalent mining height for paste-backfilling mining was 0.4 m, and so the protective layer thickness was 2.4 m. From the revised formula (Eq. 5), the height of the water-flowing fractured zone was calculated as 16.67 m, and the height of the waterproof coal (rock) pillars mined under the Quaternary groundwater and rivers was calculated as 19.07 m, which is considerably less than the normal mining height. The paste is less permeable after compaction, which also makes it an excellent anti-seepage basis for later mining of the lower 4–2 coal seam.

Numerical computational mechanical models have been developed for work faces involving mining under water, with the Moore–Cullen criterion adopted for the yield conditions (Pang et al. 2021). The total numbers of zones corresponding to the numerical models for the four sets of working faces are 154,800, 120,000, 102,000, and 116,400, respectively, and the total numbers of grid points are 165,230, 128,371, 109,306, and 124,558, respectively. The excavation part of the model is simulated by null elements, with horizontal constraints imposed on the boundaries around the model and vertical constraints imposed on the bottom boundary (Fig. 8).

The thicknesses of the intact bedrock roofs for the four sets of working faces are 57 m, 40 m, 30.83 m, and 30.38 m, respectively. From experience, the failure of the overlying strata on the working face peaks when the advancing

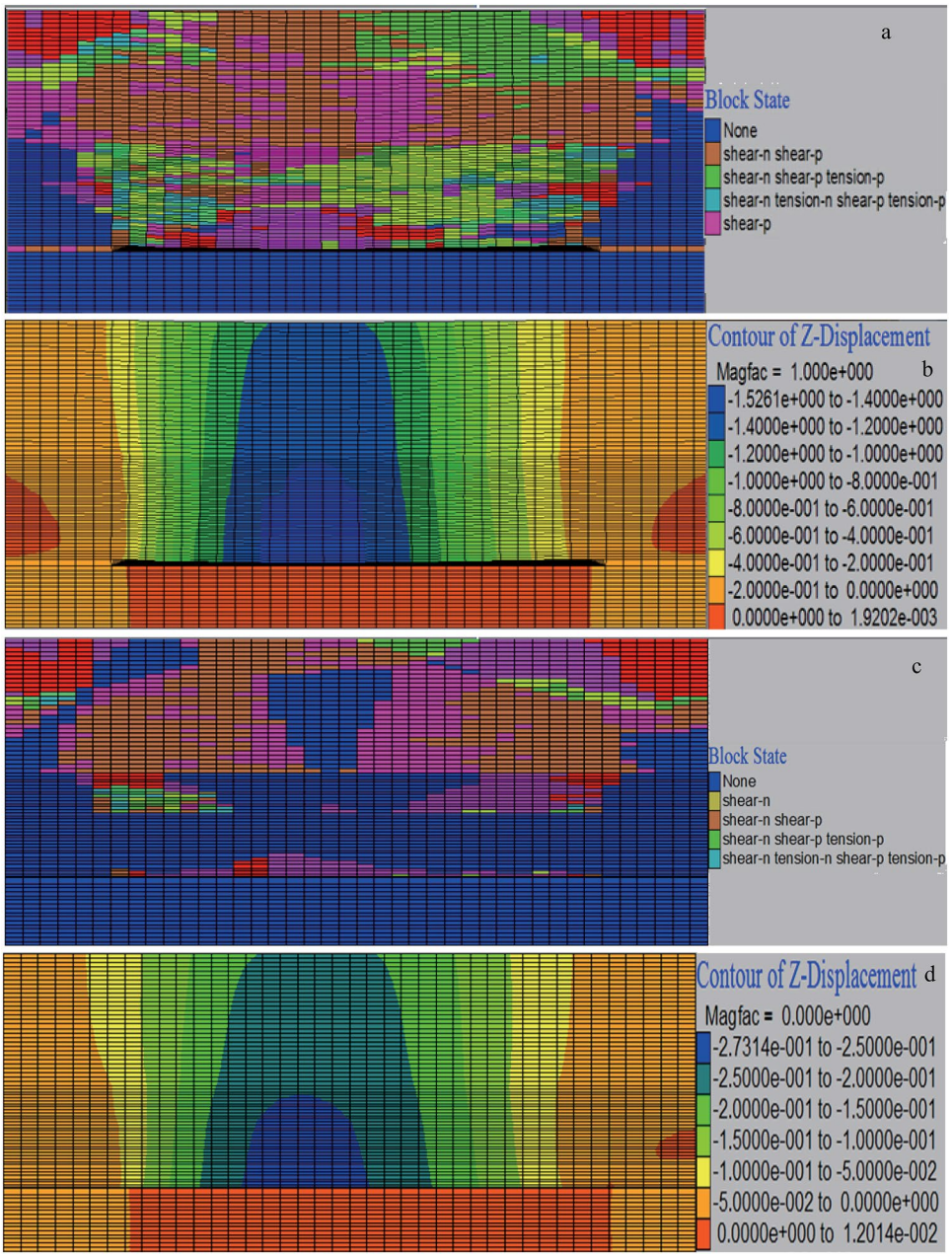

Fig. 12 Mining effects for working faces 31,218–31,220: **a** failure area of full caving; **b** vertical deformation of full caving; **c** failure area of backfill mining; **d** vertical deformation of backfill mining

distance of the mining face is the same as the width of the working face; i.e. the bedrock failure area is greatest when the working face advances to 200 m. The models of full caving have 10 m of cyclic mining footage for the four sets of working faces, and the excavations are carried out along the coal-seam floor. The average mining height is 2.9 m, 2.8 m, 3.2 m, and 2.8 m, respectively, and the filling of the four sets of working faces is done using full-backfilling. According to the theory of equivalent mining height, the average equivalent mining height is 0.4 m, the cyclic footage is 2 m, and the backfilling step is 2 m for the models. Under the same conditions, the distribution of failure area and vertical deformation after full caving and backfill mining are shown in Figs. 9, 10, 11 and 12.

Under the conditions of caving mining, when the four sets of working faces are advanced to 200 m, the fault area essentially reaches the surface, and the water-flowing fractured zone communicates with the overlying aquifer, which is prone to causing water–sand inrush in the working faces and serious mining safety hazards. The surface subsidence above the four working faces was 1–1.2 m, 0.8–1 m, 0.8–1 m, and 1.2–1.4 m, respectively. With backfill mining, when the four sets of working faces are advanced to 200 m, the heights of the water-flowing fractured zone are 17.4 m, 12 m, 10.31 m, and 10.58 m, respectively. The failure area

does not penetrate the entire bedrock of the roof and does not pose a risk of a water–sand inrush, and the surface subsidence above the four working faces is now only 0.15 m, 0.16–0.17 m, 0.2 m, and 0.27 m, respectively.

The numerical simulations show that when the backfill method is used, the height of the water-flowing fractured zone is reduced substantially, the risk of a water–sand inrush is reduced, the coal recovery is increased, the waste of coal resources is reduced, the aquifer is prevented from being destroyed, and the fragile ecological environment is protected. Paste-backfill mining is also conducive to the formation of a new waterproof roof, which lays a good foundation for mining the 4–2 coal seam under the 3–1 coal seam.

Conclusions

The research reported herein evaluated the water inrush conditions for mining the 3–1 coal seam at the Jinjie coal mine and analyzed the feasibility of safely mining under the Qingcaojiegou and Hezegou Rivers using "three maps—two predictions," the theory of equivalent mining height, and numerical simulation methods. Using the revised empirical formula, we predicted the height of the water-flowing fractured zone and then drew connectivity zoning maps of the 3–1 coal-seam roof. The results showed that part of the Quaternary aquifer and most of the J_2z aquifer are relatively high-risk areas.

We constructed a water-abundance evaluation model, calculated the weight of each control factor using AHP, and drew water-abundance zoning maps. The results showed that there are large areas of strong or relatively strong water abundance in the 3–1 coal-seam roof. A comprehensive zoning map of roof water inrush conditions was obtained by superimposing the connectivity zoning map and the water-abundance zoning map, with five levels of water inrush risk. The results showed that large areas of the second, third, and fourth panels of the coalfield are at high or low risk and face a serious threat of roof water inrush.

Using the theory of equivalent mining height and numerical simulation, we analyzed the feasibility of safely mining with backfilling under the rivers. The results showed that the failure zone formed while backfill mining does not completely penetrate the bedrock of the roof, and therefore should not cause a water–sand inrush.

Supplementary Information The online version contains supplementary material available at https://doi.org/10.1007/s10230-023-00939-1.

Acknowledgements This research was financially supported by the National Key R&D Program of China (2021YFC2902004), the China National Natural Science Foundation (42072284, 42027801, 41877186), the Fundamental Research Funds for the Central Universities (2022YQSH01, 2022YJSSH01). The authors also thank the editor and reviewers for their helpful suggestions.

Data availability The data that support the findings of this study are available on request from the corresponding author, upon reasonable request.

References

Aditian A, Kubota T, Shinohara Y (2018) Comparison of GIS-based landslide susceptibility models using frequency ratio, logistic regression, and artificial neural network in a tertiary region of Ambon, Indonesia. Geomorphology 318:101–111. https://doi.org/10.1016/j.geomorph.2018.06.006

Bai EH, Guo WB, Tan Y (2019) Negative externalities of high-intensity mining and disaster prevention technology in China. Bull Eng Geol Environ 78:5219–5235. https://doi.org/10.1007/s10064-019-01468-4

Bergado DT, Teerawattanasuk C (2008) 2D and 3D numerical simulations of reinforced embankments on soft ground. Geotext Geomembr 26:39–55. https://doi.org/10.1016/j.geotexmem.2007.03.003

Booth CJ, Bertsch LP (2002) Groundwater geochemistry in shallow aquifers above longwall mines in Illinois, USA. Hydrogeol J 7:561–575. https://doi.org/10.1007/s100400050229

Booth CJ, Curtiss AM, Demaris PJ, Bauer RA (2000) Site-specific variation in the potentiometric response to subsidence above active longwall mining. Environ Eng Geosci 6:383–394. https://doi.org/10.2113/gseegeosci.6.4.383

Chen SJ, Yin DW, Cao FW, Liu Y, Ren KQ (2016) An overview of integrated surface subsidence-reducing technology in mining areas of China. Nat Hazards 81:1129–1145. https://doi.org/10.1007/s11069-015-2123-x

El-Nashaar A, Fathy A, Zeedan A, Al-Ahwany A, Shamloul R (2006) Validity and reliability of the Arabic version of the National Institutes of Health Chronic Prostatitis Symptom Index. Urol Int 77:227–231. https://doi.org/10.1159/000094814

Esterhuizen GS, Dolinar DR, Ellenberger JL (2011) Pillar strength in underground stone mines in the United States. Int J Rock Mech Min 48:42–50. https://doi.org/10.1016/j.ijrmms.2010.06.003

Fan L (2005) Discussing on coal mining under water-containing condition. Coal Geol Explor 33:53–56 (**in Chinese**)

Flatley A, Markham A (2021) Establishing effective mine closure criteria for river diversion channels. J Environ Manag 287:112287. https://doi.org/10.1016/j.jenvman.2021.112287

Gui HR, Lin ML (2016) Types of water hazards in China coalmines and regional characteristics. Nat Hazards 84:1501–1512. https://doi.org/10.1007/s11069-016-2488-5

Guo GL, Zhu XJ, Zha JF, Wang Q (2014) Subsidence prediction method based on equivalent mining height theory for solid backfilling mining. Trans Nonferrous Met Soc China 24:3302–3308. https://doi.org/10.1016/S1003-6326(14)63470-1

Islam MR, Hayashi D, Kamruzzaman ABM (2009) Finite element modeling of stress distributions and problems for multi-slice longwall mining in Bangladesh, with special reference to the Barapukuria coal mine. Int J Coal Geol 78:91–109. https://doi.org/10.1016/j.coal.2008.10.006

Ji JS, Li ZH, Yang K, Zhou GH, Ma GJ, Liu C, Zhou P (2022) Research on formation mechanism and evolution pattern of bed separation zone during repeated mining in multiple coal seams. Geofluids. https://doi.org/10.1155/2022/4290063

Kazakis N, Voudouris KS (2015) Groundwater vulnerability and pollution risk assessment of porous aquifers to nitrate: modifying the DRASTIC method using quantitative parameters. J Hydrol 525:13–25. https://doi.org/10.1016/j.jhydrol.2015.03.035

Kim J-M, Parizek RR, Elsworth D (1997) Evaluation of fully-coupled strata deformation and groundwater flow in response to longwall mining. Int J Rock Mech Min 34:1187–1199. https://doi.org/10.1016/s1365-1609(97)80070-6

Li B, Wu Q (2019) Catastrophic evolution of water inrush from a water-rich fault in front of roadway development: a case study of the Hongcai coal mine. Mine Water Environ 38:421–430. https://doi.org/10.1007/s10230-018-00584-z

Li J, Feng C, Zhu XG, Zhang YM (2022) Analysis of the coal fluidization mining process with the continuous-discontinuous coupled particle-block method. Geofluids. https://doi.org/10.1155/2022/7001654

Lv XJ, Xiao W, Zhao YL, Zhang WK, Li SC, Sun HX (2019) Drivers of spatio-temporal ecological vulnerability in an arid, coal mining region in western China. Ecol Indic. https://doi.org/10.1016/j.ecolind.2019.105475

Mase T, Hashiguchi K (2009) Numerical analysis of footing settlement problem by subloading surface model. Soils Found 49:207–220. https://doi.org/10.3208/sandf.49.207

Miao X, Qian M (2009) Research on green mining of coal resources in China: current status and future prospects. J Min Safe Eng 26:1–14 (**in Chinese**)

Mu WP, Wu X, Deng RC, Hao Q, Qian C (2020) Mechanism of water inrush through fault zones using a coupled fluid-solid numerical model: a case study in the Beiyangzhuang coal mine, northern China. Mine Water Environ 39:380–396. https://doi.org/10.1007/s10230-020-00689-4

Pang LF, Liu WT, Zheng QS, Du YH, Meng XX, Li X (2021) Evaluation and analysis of metal mine filling based on numerical simulation and actual measurement. Environ Earth Sci. https://doi.org/10.1007/s12665-021-09844-8

Qian M, Miao X, Xu J (1996) Theoretical study of key stratum in ground control. J China Coal Soc, 21:2–7 (**in Chinese**)

Rajeev P, Kodikara J (2011) Numerical analysis of an experimental pipe buried in swelling soil. Comput Geotech 38:897–904. https://doi.org/10.1016/j.compgeo.2011.06.005

Roy J, Saha S, Arabameri A, Blaschke T, Bui DT (2019) A novel ensemble approach for landslide susceptibility mapping (LSM) in Darjeeling and Kalimpong Districts, West Bengal, India. Remote Sens. https://doi.org/10.3390/rs11232866

Saaty TL (1977) A scaling method for priorities in hierarchical structures. J Math Psych 15:234–281. https://doi.org/10.1016/0022-2496(77)90033-5

Shen J (2017) Mining mode and engineering application for "Coal-Water" dual-resources mine under the threat of roof water hazard. China Univ of Mining and Technology, Beijing (**in Chinese**)

State Administration of Work Safety NCMSA, National Energy Administration, National Railway Administration of the People's Republic of China (2017) Specification for Coal Pillar Retention and Coal Mining in Buildings, Water, Railways and Main Roadways

Wang CJ, Lei SG, Elmore AJ, Jia D, Mu SG (2019) Integrating temporal evolution with cellular automata for simulating land cover change. Remote Sens. https://doi.org/10.3390/rs11030301

Wen JH, Cheng WM, Chen LJ, Shi SS, Wen ZJ (2019) A study of the dynamic movement rule of overlying strata combinations using a short-wall continuous mining and full-caving method. Energy Sci Eng 7:2984–3004. https://doi.org/10.1002/ese3.474

Wu Q, Li D (2009) Research of "Coal-water" double-resources mine construction and development. Coal Geol China 21:32–35+62 (**in Chinese**)

Wu Q, Liu Y, Zhou W, Wu X, Liu S, Sun W, Zeng Y (2015a) Assessment of water inrush vulnerability from overlying aquifer using GIS-AHP-based "three maps-two predictions" method: a case study in Hulusu coal mine, China. Q J Eng Geol Hydrogeol 48:234–243. https://doi.org/10.1144/qjegh2015-014

Wu Q, Liu YZ, Zhou WF, Li BY, Zhao B, Liu SQ, Sun WJ, Zeng YF (2015b) Evaluation of water inrush vulnerability from aquifers overlying coal seams in the Menkeqing Coal Mine, China. Mine Water Environ 34:258–269. https://doi.org/10.1007/s10230-014-0313-5

Yang Q, Wang L, Ma H, Yu K, Martin JD (2016) Hydrochemical characterization and pollution sources identification of groundwater in Salawusu aquifer system of Ordos Basin, China. Environ Pollut 216:340–349. https://doi.org/10.1016/j.envpol.2016.05.076

Zeng Y, Liu S, Zhang W, Zhai Y (2016) Application of artificial neural network technology to predicting small faults and folds in coal seams, China. Sustain Water Resour Manag 2:175–181. https://doi.org/10.1007/s40899-016-0054-7

Zeng Y, Wu Q, Liu S, Zhai Y, Lian H, Zhang W (2017) Evaluation of a coal seam roof water inrush: case study in the Wangjialing coal mine, China. Mine Water Environ 37:174–184. https://doi.org/10.1007/s10230-017-0459-z

Zeng YF, Pang ZZ, Wu Q, Hua ZL, Lv Y, Wang L, Zhang Y, Du X, Liu SQ (2022) Study of water-controlled and environmentally friendly coal mining models in an ecologically fragile area of northwest China. Mine Water Environ 41:802–816. https://doi.org/10.1007/s10230-022-00871-w

Zeng Y, Meng S, Wu Q, Mei A, Bu W (2023) Ecological water security impact of large coal base development and its protection. J Hydrol. https://doi.org/10.1016/j.jhydrol.2023.129319

Zhang Q, Xu CY, Zhang ZX, Chen YD (2009) Changes of temperature extremes for 1960–2004 in far-west China. Stoch Environ Res Risk Assess 23:721–735. https://doi.org/10.1007/s00477-008-0252-4

Zhang JX, Zhang Q, Sun Q, Gao R, Germain D, Abro S (2015) Surface subsidence control theory and application to backfill coal mining technology. Environ Earth Sci 74:1439–1448. https://doi.org/10.1007/s12665-015-4133-0

Zhang JX, Deng XJ, Zhao X, Ju F, Li BY (2016) Effective control and performance measurement of solid waste backfill in coal mining. Int J Min Reclam Environ 31:91–104. https://doi.org/10.1080/17480930.2015.1120384

Zhang Q, Zhou G, Qian X, Yuan M, Sun Y, Wang D (2018) Diffuse pollution characteristics of respirable dust in fully-mechanized mining face under various velocities based on CFD investigation. J Clean Prod 184:239–250. https://doi.org/10.1016/j.jclepro.2018.02.230

Zhao D, Zeng YF, Wu Q, Du X, Gao S, Mei AS, Zhao HN, Zhang ZH, Zhang XH (2022a) Source discrimination of mine gushing water using self-organizing feature maps: a case study in Ningtiaota Coal Mine, Shaanxi, China. Sustainability. https://doi.org/10.3390/su14116551

Zhao D, Zeng YF, Wu Q, Mei AS, Gao S, Du X, Yang WH (2022b) Hydrogeochemical characterization and suitability assessment of groundwater in a typical coal mining subsidence area in China using self-organizing feature map. Environ Earth Sci 81:17. https://doi.org/10.1007/s12665-022-10596-2

Zhao Z, Wu P, Wang L, Li M, Mao XB, Chen L (2022c) Influence of moisture content on creep mechanical characteristic and mic-fracture behavior of water-bearing coal specimen. Geofluids. https://doi.org/10.1155/2022/4014462

Zheng KD, Xuan DY, Li J (2022) Study on fluid-solid characteristics of grouting filling similar-simulation materials. Minerals. https://doi.org/10.3390/min12050502

Zhou G, Zhang Q, Bai R, Fan T, Wang G (2017) The diffusion behavior law of respirable dust at fully mechanized caving face in coal mine: CFD numerical simulation and engineering application. Proc Saf Environ Prot 106:117–128. https://doi.org/10.1016/j.psep.2016.12.005

Zhou X, Chen W, Wang YN, Zhang DJ, Wang Q, Zhao MJ, Xia XL (2019) Suitability evaluation of large-scale farmland transfer on the loess plateau of northern Shaanxi, China. Land Degrad Dev 30:1258–1269. https://doi.org/10.1002/ldr.3313

Zhu L, Song TQ, Gu WZ, Xu K, Liu ZC, Qiu FQ, Zhang XF (2022) Study on layered-backfill-based water protection technology of thick coal seam in the ecologically fragile mining area in western China. Geofluids. https://doi.org/10.1155/2022/3505176